



Pulsating Tubules from Noncovalent Macrocycles

Zhegang Huang *et al.*
Science **337**, 1521 (2012);
DOI: 10.1126/science.1224741

This copy is for your personal, non-commercial use only.

If you wish to distribute this article to others, you can order high-quality copies for your colleagues, clients, or customers by [clicking here](#).

Permission to republish or repurpose articles or portions of articles can be obtained by following the guidelines [here](#).

The following resources related to this article are available online at www.sciencemag.org (this information is current as of November 6, 2013):

Updated information and services, including high-resolution figures, can be found in the online version of this article at:

<http://www.sciencemag.org/content/337/6101/1521.full.html>

Supporting Online Material can be found at:

<http://www.sciencemag.org/content/suppl/2012/09/19/337.6101.1521.DC1.html>

A list of selected additional articles on the Science Web sites **related to this article** can be found at:

<http://www.sciencemag.org/content/337/6101/1521.full.html#related>

This article **cites 35 articles**, 6 of which can be accessed free:

<http://www.sciencemag.org/content/337/6101/1521.full.html#ref-list-1>

This article has been **cited by** 1 articles hosted by HighWire Press; see:

<http://www.sciencemag.org/content/337/6101/1521.full.html#related-urls>

This article appears in the following **subject collections**:

Chemistry

<http://www.sciencemag.org/cgi/collection/chemistry>

deposition of the second SAM component over 12 hours; sharp pattern features were produced even in this case, arguing against diffusion or dissolution of the original lift-off pattern.

We investigated the time needed for the contact-induced chemical reaction at the stamp-substrate interface by examining 1-min versus 5-min contact times between oxygen plasma-treated PDMS stamps and hydroxyl-terminated, alkanethiol-coated Au surfaces. Features were transferred even with 1-min contact times; however, shorter contact times resulted in poor features produced after wet etching. Additionally, pattern transfer was maintained with short SAM deposition times. Hydroxyl-terminated alkanethiol SAMs formed during 1 hour of deposition were found to provide good transfer of stamp features to Au substrates, comparable to transfer obtained from SAMs formed overnight. These findings demonstrate advantages associated with short contact and SAM formation times for facilitating robust, expeditious, and high-throughput patterning by CLL. Ultimately, limits for SAM deposition and stamp contacts times will depend on the specific molecules used for SAM formation.

With this method, conventional nanolithographic patterning techniques such as photolithography and electron-beam lithography need only be used for the fabrication of stamp master molds. Once individual masters are produced, CLL can be implemented as a strategy for high-resolution, high-throughput, low-cost pattern fabrication. Because CLL enables patterns to be transferred to underlying substrates and can be used in a multiple-stamping strategy to produce patterns that are smaller than the actual stamp features, possible applications of CLL include the production of high-fidelity nanometer-scale patterns on Au substrates, as well as patterning of different materials such as Si, Ge, Pd, Pt, and graphene.

References and Notes

- B. D. Gates *et al.*, *Chem. Rev.* **105**, 1171 (2005).
- C. G. Willson, B. J. Roman, *ACS Nano* **2**, 1323 (2008).
- H. M. Saavedra *et al.*, *Rep. Prog. Phys.* **73**, 036501 (2010).
- W. Shim *et al.*, *Nature* **469**, 516 (2011).
- R. D. Piner, J. Zhu, F. Xu, S. H. Hong, C. A. Mirkin, *Science* **283**, 661 (1999).
- S. Xu, P. E. Laibinis, G. Y. Liu, *J. Am. Chem. Soc.* **120**, 9356 (1998).
- S. Xu, G. Y. Liu, *Langmuir* **13**, 127 (1997).
- Y. N. Xia, G. M. Whitesides, *Angew. Chem. Int. Ed.* **37**, 550 (1998).
- X. M. Li, M. Peter, J. Huskens, D. N. Reinhoudt, *Nano Lett.* **3**, 1449 (2003).
- J. A. Rogers, R. G. Nuzzo, *Mater. Today* **8**, 50 (2005).
- J. L. Wilbur, A. Kumar, E. Kim, G. M. Whitesides, *Adv. Mater.* **6**, 600 (1994).
- S. Y. Chou, P. R. Krauss, P. J. Renstrom, *Science* **272**, 85 (1996).
- Y. L. Loo *et al.*, *J. Vac. Sci. Technol. B* **20**, 2853 (2002).
- W. R. Childs, R. G. Nuzzo, *J. Am. Chem. Soc.* **124**, 13583 (2002).
- A. Kumar, G. M. Whitesides, *Appl. Phys. Lett.* **63**, 2002 (1993).
- K. L. Christman, V. D. Enriquez-Rios, H. D. Maynard, *Soft Matter* **2**, 928 (2006).
- A. Vaish, M. J. Shuster, S. Cheunkar, P. S. Weiss, A. M. Andrews, *Small* **7**, 1471 (2011).
- M. J. Shuster *et al.*, *Chem. Commun.* **47**, 10641 (2011).
- J. M. McLellan, M. Geissler, Y. N. Xia, *J. Am. Chem. Soc.* **126**, 10830 (2004).
- C. Srinivasan *et al.*, *ACS Nano* **1**, 191 (2007).
- A. B. Braunschweig, F. Huo, C. A. Mirkin, *Nat. Chem.* **1**, 353 (2009).
- S. Xu, S. Miller, P. E. Laibinis, G. Y. Liu, *Langmuir* **15**, 7244 (1999).
- R. C. Tiberio *et al.*, *Appl. Phys. Lett.* **62**, 476 (1993).
- Y. L. Loo, R. L. Willett, K. W. Baldwin, J. A. Rogers, *J. Am. Chem. Soc.* **124**, 7654 (2002).
- J. Lahiri, E. Ostuni, G. M. Whitesides, *Langmuir* **15**, 2055 (1999).
- C. Donzel *et al.*, *Adv. Mater.* **13**, 1164 (2001).
- T. Kaufmann, B. J. Ravoo, *Polym. Chem.* **1**, 371 (2010).
- S. R. Wasserman, H. Biebuyck, G. M. Whitesides, *J. Mater. Res.* **4**, 886 (1989).
- S. J. Stranick, A. N. Parikh, D. L. Allara, P. S. Weiss, *J. Phys. Chem.* **98**, 11136 (1994).
- S. J. Stranick *et al.*, *Nanotechnology* **7**, 438 (1996).
- H. Skulason, C. D. Frisbie, *J. Am. Chem. Soc.* **122**, 9750 (2000).
- M. Liu, N. A. Amro, G. Y. Liu, *Annu. Rev. Phys. Chem.* **59**, 367 (2008).
- G. E. Poirier, M. J. Tarlov, *Langmuir* **10**, 2853 (1994).
- G. E. Poirier, M. J. Tarlov, *J. Phys. Chem.* **99**, 10966 (1995).
- P. Maksymovych, D. C. Sorescu, J. T. Yates Jr., *Phys. Rev. Lett.* **97**, 146103 (2006).
- M. Yu *et al.*, *Phys. Rev. Lett.* **97**, 166102 (2006).
- A. M. Moore *et al.*, *J. Am. Chem. Soc.* **129**, 10352 (2007).
- P. Han *et al.*, *ACS Nano* **3**, 3115 (2009).
- When oxygen plasma treatment was omitted, a featureless PDMS stamp brought into contact with a hydroxyl-terminated, SAM-coated Au surface failed to produce XPS signature peaks indicative of Au lift-off (fig. S2). Likewise, stamps that were either treated with oxygen plasma or left untreated but not subjected to the lift-off process had no indication of Au on the stamp surfaces (figs. S3 and S4, respectively).
- H. L. Gou, J. J. Xu, X. H. Xia, H. Y. Chen, *ACS Appl. Mater. Interfaces* **2**, 1324 (2010).
- O. J. A. Schueller, D. C. Duffy, J. A. Rogers, S. T. Brittain, G. M. Whitesides, *Sens. Actuators A* **78**, 149 (1999).
- D. C. Duffy, O. J. A. Schueller, S. T. Brittain, G. M. Whitesides, *J. Micromech. Microeng.* **9**, 211 (1999).
- H. M. Saavedra, C. M. Thompson, J. N. Hohman, V. H. Crespi, P. S. Weiss, *J. Am. Chem. Soc.* **131**, 2252 (2009).
- W. S. Liao, X. Chen, J. Chen, P. S. Cremer, *Nano Lett.* **7**, 2452 (2007).
- M. Geissler *et al.*, *Langmuir* **19**, 6301 (2003).
- K. L. Prime, G. M. Whitesides, *Science* **252**, 1164 (1991).
- A. A. Dameron *et al.*, *Nano Lett.* **5**, 1834 (2005).
- S. J. Stranick, M. M. Kamna, P. S. Weiss, *Surf. Sci.* **338**, 41 (1995).

Acknowledgments: Supported by U.S. Department of Energy grant DOE-FG02-10ER46734, NSF grant CHE-1013042, and the Kavli Foundation. S.C. thanks the government of Thailand for a graduate fellowship. We thank D. L. Allara, J. N. Hohman, and S. A. Claridge for helpful discussions; A. Nel for the use of his fluorescence microscope; the California NanoSystems Institute Nano and Pico Characterization Facility; and S. Rujikietgumjorn for help in image processing.

Supplementary Materials

www.sciencemag.org/cgi/content/full/337/6101/1517/DC1
Materials and Methods
Supplementary Text
Figs. S1 to S8
References (49, 50)

12 March 2012; accepted 1 August 2012
10.1126/science.1221774

Pulsating Tubules from Noncovalent Macrocycles

Zhegang Huang,^{1,3} Seong-Kyun Kang,¹ Motonori Banno,² Tomoko Yamaguchi,² Dongseon Lee,¹ Chaok Seok,¹ Eiji Yashima,² Myongssoo Lee^{1*}

Despite recent advances in synthetic nanometer-scale tubular assembly, conferral of dynamic response characteristics to the tubules remains a challenge. Here, we report on supramolecular nanotubules that undergo a reversible contraction-expansion motion accompanied by an inversion of helical chirality. Bent-shaped aromatic amphiphiles self-assemble into hexameric macrocycles in aqueous solution, forming chiral tubules by spontaneous one-dimensional stacking with a mutual rotation in the same direction. The adjacent aromatic segments within the hexameric macrocycles reversibly slide along one another in response to external triggers, resulting in pulsating motions of the tubules accompanied by a chiral inversion. The aromatic interior of the self-assembled tubules encapsulates hydrophobic guests such as carbon-60 (C₆₀). Using a thermal trigger, we could regulate the C₆₀-C₆₀ interactions through the pulsating motion of the tubules.

Self-assembly of small molecular modules into tubules with hollow cavities is a key structural feature of living systems, as exemplified by tobacco mosaic virus and cytoplas-

mic microtubules (1, 2). Inspired by the biological systems, numerous efforts have been devoted to the design of synthetic building blocks that can form such hollow nanostructures through orchestrated interplay of various noncovalent interactions (3). Synthetic tubules have previously been fashioned by self-assembly of lipid molecules (4), aromatic amphiphiles (5–9), and oligopeptides (10–12). The stacking of ring-shaped compounds is an alternative way to construct tubular structures (13, 14). An example is provided by doughnut-like toroidal proteins that stack on top of one

¹Department of Chemistry, Seoul National University, Seoul 151-747, Korea. ²Department of Molecular Design and Engineering, Graduate School of Engineering, Nagoya University, Chikusa-ku, Nagoya 464-8603, Japan. ³Department of Chemistry, Harbin Institute of Technology, Harbin, 150001, P. R. China.

*To whom correspondence should be addressed. E-mail: myongssoo@snu.ac.kr

These observations, together with inspection of CPK models, indicate that **1** self-assembles via a fully overlapped packing arrangement into the hexameric macrocycles, which, in turn, stack on top of each other with mutual rotation in a single direction to form helical tubules.

We envisioned that introduction of a pyridine unit on the concave side of the apex of the bent-shaped aromatic segment might induce adjacent molecules to slide into a looser packing arrangement because pyridine is well-known to form water clusters through hydrogen bonding (18, 19). In this context, we prepared **2a** containing a pyridine unit at its valley position. DLS experiments with dilute aqueous solutions (0.002 wt %) indicated formation of discrete aggregates with a diameter of ~12 nm (fig. S3A). The aggregate structure was visualized by TEM (Fig. 1D). When the sample was cast from the solution and then negatively stained with uranyl acetate, the image showed toroidal objects with a uniform diameter of 11 nm and an internal cavity 4 nm in diameter. To further confirm the formation of the toroids, we performed atomic force microscopy (AFM) measurements of the samples prepared by drop casting of the aqueous solution (0.002 wt %) on a mica surface (fig. S3C). The image clearly revealed toroidal objects 3.4 Å in height, demonstrating that the toroidal objects are single stacks of the hexameric macrocycles. In great contrast to **1**, the absorption maximum of **2a** in water is red-shifted and the fluorescence intensity apparently enhanced with respect to those observed in chloroform solutions, indicative of *J*-type stacking of the aromatic segments (Fig. 1E) (20). All these observations indicate that **2a** self-assembles into expanded hexameric macrocycles through a

slipped packing arrangement between the aromatic segments. The expansion of the noncovalent macrocycles is reflected in increased dimensions of both external and internal diameters compared with that of **1** (Fig. 1D). This expansion of the hexameric macrocycles could be explained by considering the formation of water clusters at the pyridine unit of the *v*-position of **2a**. To corroborate the formation of water clusters at the pyridine unit, we prepared model compound **7a** (2,6-dibromo pyridine derivative). Proton nuclear magnetic resonance (¹H-NMR) measurements of **7a** showed that the proton signals associated with the pyridine are downfield-shifted when the solvent is changed from CDCl₃ to D₂O/H₂O, indicating the formation of hydrogen bonds with H₂O at the pyridine unit (fig. S3E). The water cluster enforces slipping of adjacent aromatic segments into a looser packing arrangement to reduce steric crowding at the valley position of the internal cavity. The sliding motion between the adjacent aromatic segments gives rise to the formation of the expanded hexameric macrocycles with an increase in external diameter from 7 to 11 nm.

The expanded macrocycles undergo supramolecular polymerization with increasing concentration by stacking on top of each other with mutual rotation in the same direction to form elongated helical tubules. DLS measurements showed that hydrodynamic radius increases, with increasing concentration within this range of concentration (fig. S4A). The TEM image of the solution with a concentration of 0.02 wt % revealed the formation of elongated tubules with an external diameter of 11 nm and internal diameter of 4 nm (Fig. 2B, fig. S5A). These results demon-

strate that the diameters of the hexameric macrocycles are conserved even after supramolecular polymerization. This is also reflected in the unaltered optical spectroscopic features after transformation into the tubules; that is, preservation of the slipped packing arrangement of the aromatic segments (fig. S4C). CD spectra show increased intensity with increasing concentration, indicative of helical stacking of the macrocycles with a preferred handedness (Fig. 2A). Assemblies derived from the enantiomer **2b** display opposite CD signals with a mirror-image relationship (fig. S4D), indicating that the molecular chirality is transferred to the self-assembled structure (21, 22).

The formation of hollow tubules with oligoether dendritic exterior and pyridine interior suggested that aqueous solutions of **2a** would exhibit thermoresponsive behavior, because the ethylene oxide chains and the pyridine units undergo thermally regulated dehydration upon heating (23). This dehydration was confirmed by temperature-dependent ¹H-NMR measurements with a reference **7a** (fig. S5C). The resonances associated with pyridine units shifted upfield, and those of the ethylene oxide chains broadened, together with a decrease in intensity upon heating above 55°C, clearly demonstrating the loss of hydrogen bonding interactions between pyridine nitrogens or ether oxygens and water molecules. The dehydration process could allow sliding of the aromatic segments from the slipped arrangement into the fully overlapped motif to maximize aromatic π - π stacking interactions. This packing consideration is reflected in the blue-shifted absorption maximum and fluorescence quenching upon heating (fig. S6, A and C). We believe

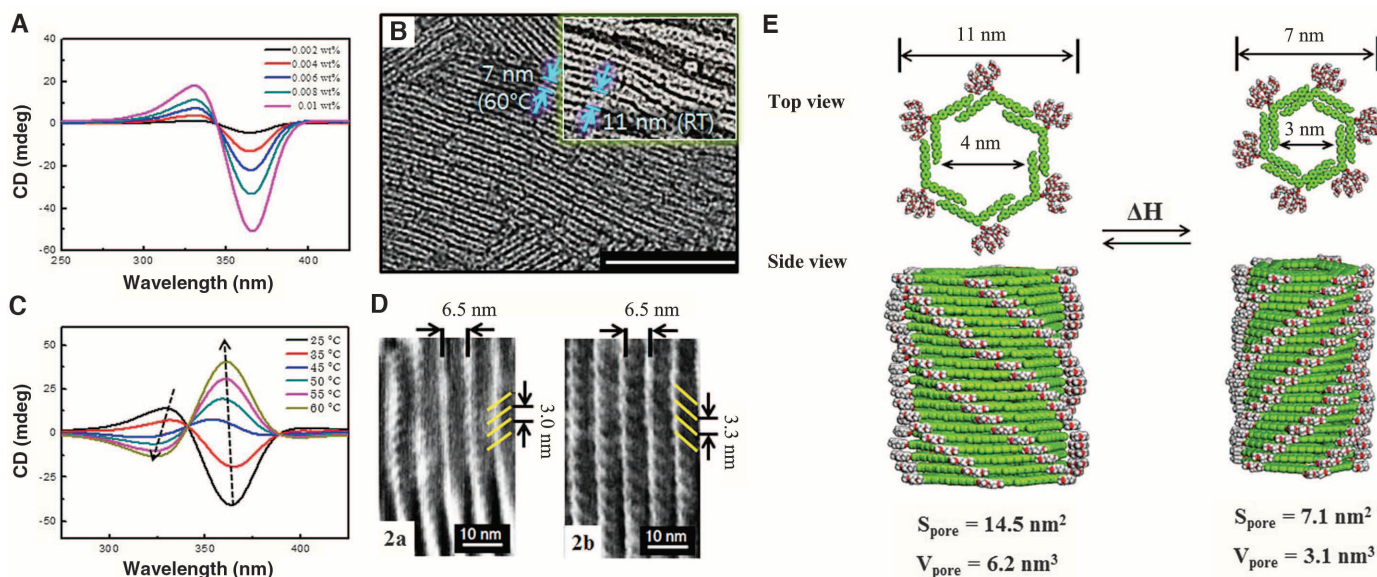


Fig. 2. (A) CD spectra of **2a** in aqueous solution at various concentrations. (B) TEM image of **2a** from 0.01 wt % aqueous solution prepared at 60°C (scale bar, 100 nm) (Inset) Prepared at room temperature. (C) Temperature-dependent CD spectra of **2a** (0.01 wt %) in aqueous solution. (D) AFM phase images (scale = 60 by 35 nm) of 2D self-assembled right-

handed **2a** (left) and left-handed **2b** (right) on HOPG. (E) Schematic representation of reversible switching of the tubules between expanded and contracted states with chirality inversion. S_{pore} , cross-sectional area of hollow pore in a slice of the macrocycles; V_{pore} , volume of hollow pore in a slice of the macrocycles.

that the observed spectral changes are the result of a fully overlapped *H*-type packing arrangement of the aromatic segments (20). To confirm this molecular rearrangement upon heating of the tubular structure, we carried out TEM experiments. On heating to 60°C, the tubular structure was retained (Fig. 2B). However, the diameter drastically decreased upon heating. The density profile taken perpendicular to the long axis of the tubule showed the external and internal diameters to be 7 and 3 nm, respectively, indicative of a 47% reduction in cross-sectional area of the internal cavity with respect to that at room temperature (fig. S5, A and B). This size change, together with all the spectral changes, is fully reversible on cooling and subsequent heating cycles. We conclude from these experimental results that this reversible contraction of the tubules results from the molecular rearrangement through

a sliding motion between the adjacent aromatic segments.

Notably, this expansion-contraction motion of the tubules is accompanied by chirality inversion (Fig. 2C). The CD spectrum of **2a** showed a strong signal with a negative Cotton effect at 369 nm, the absorption wavelength of the aromatic unit, indicating the formation of a helical superstructure with a preferred handedness. Upon heating, however, the CD signal was inverted from the negative minimum to a strong positive Cotton effect, indicating that the helical sense switches to opposite-handedness (24, 25). The CD signal with a negative minimum decreases gradually up to 45°C and is completely reversed to a positive Cotton effect upon further heating. The maximum wavelength was blue-shifted, and the maximum intensity of the CD signal was identical but with an opposite Cotton effect from

the room temperature signal, demonstrating that the tubules have highly dynamic helicities in response to temperature (fig. S7A). This positive Cotton effect is the same as that in the temperature-independent CD signal of **1**, suggesting that the tubule of **2a** at higher temperatures adopts the same sense of helicity as **1** (fig. S7C). This result demonstrates that the hexameric macrocycles stack in the identical helical sense when they are based on fully overlapped arrangements of the aromatic segments (*H*-type packing).

To corroborate the handedness of the helical tubules, we performed AFM experiments with **2a** and **2b** on highly oriented pyrolytic graphite (HOPG) in the completely dried state. The images revealed bundles of rod-like aggregates with a diameter of ~7 nm (fig. S8), suggesting that the rods on the HOPG surface correspond to the contracted tubules derived from the *H*-type aggregate

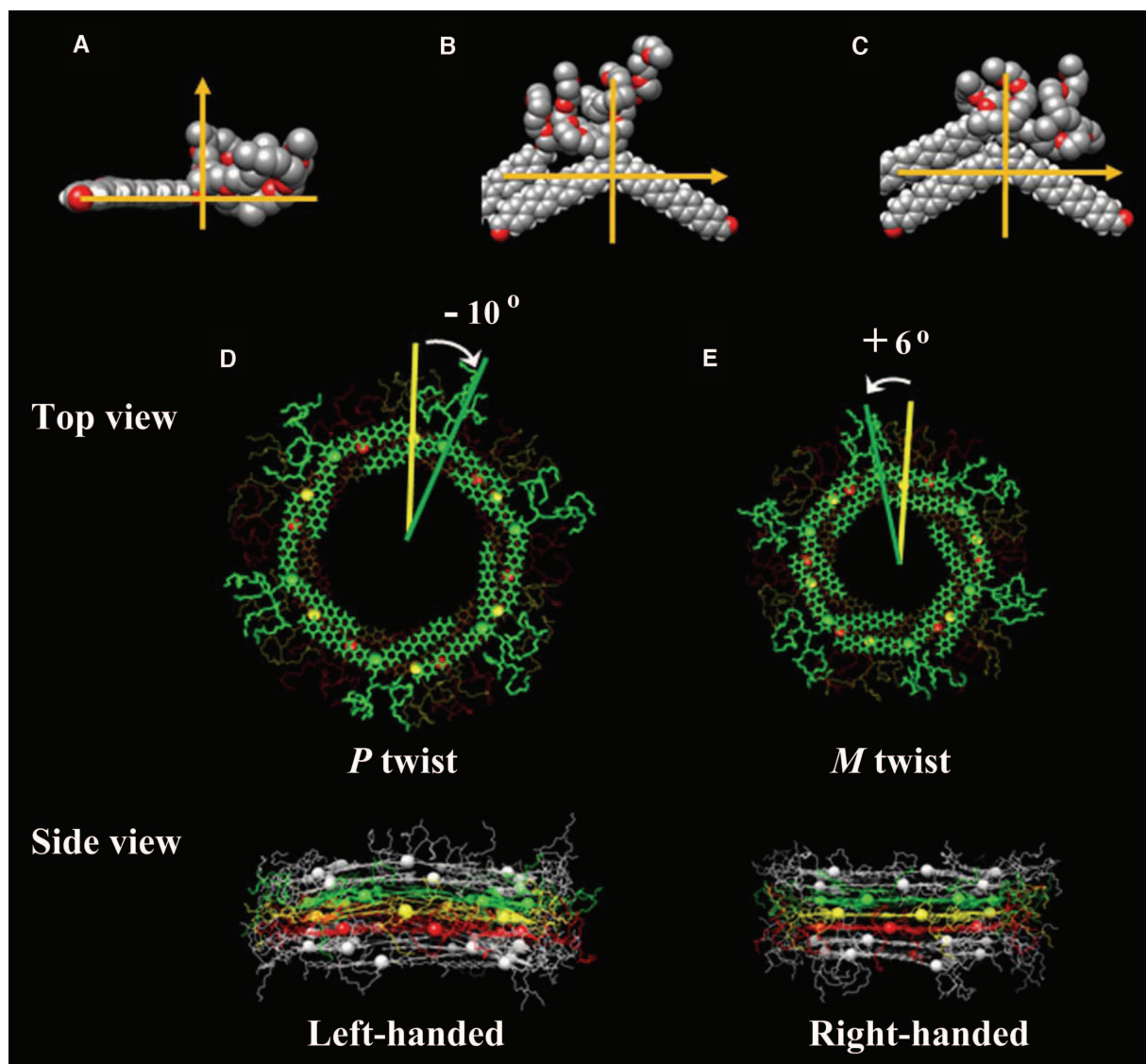


Fig. 3. Molecular dynamics simulations. (A to C) Orientation of the dendritic coil in (A) the helical axis plane, (B) the macrocyclic plane of the expanded state, and (C) the macrocyclic plane of the contracted state. (D and E) Rep-

resentative images of top and side views of the (D) expanded and (E) contracted forms of helical tubules obtained from the simulations. Pyridine nitrogen atoms are represented as colored spheres.

gation in aqueous solution. Indeed, the solution CD signals observed at room temperature inverted to opposite signs upon complete drying (fig. S9). The magnified image of tubules comprising **2a** (Fig. 2D, left) revealed a right-handed helical structure with a pitch of 3 nm that is the mirror image of the tubules comprising **2b** (Fig. 2D, right). This mirror image relationship is consistent with the CD results. In contrast with contracted tubules on HOPG, elongated objects with a diameter of 11 to 12 nm probably corresponding to the expanded state (*J*-type packing) were observed when aqueous solutions of **2a** and **2b** were cast on hydrophilic mica substrates. Although we had difficulty observing clean helical structures on the objects, most likely due to their soft and hydrated surfaces, the mirror-image helices formed through the enantiomers in the expanded state were also observed in part (fig. S10, C and D).

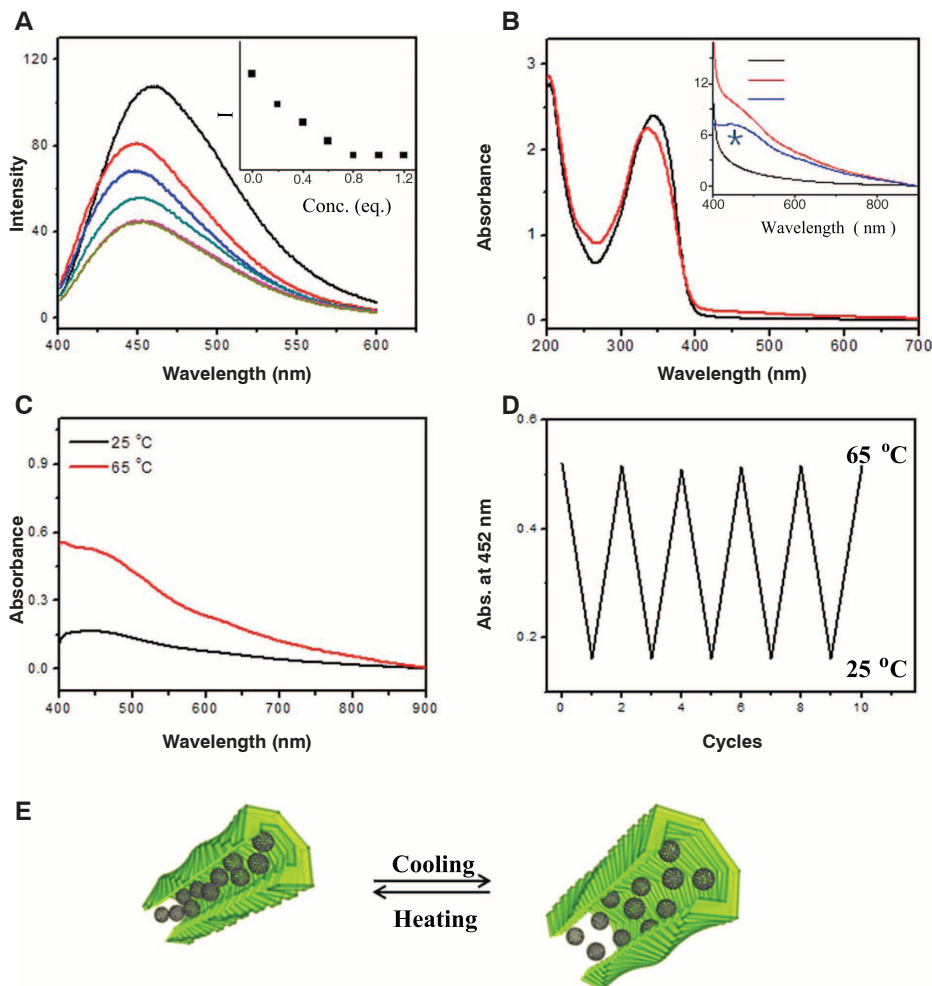
Molecular dynamics simulations of **2a** using the GROMACS 4 program supported attribution of the chirality inversion to an orientational change with temperature of the dendritic chains on the tubule exterior (Fig. 3). According to the calculations, the expanded macrocycles stack on top of each other with mutual rotations at an angle of -10° in the same direction to give

rise to left-handed helical tubules, whereas the contracted macrocycles twist $+6^\circ$ to give right-handedness (Fig. 3). The observed inversion of helical handedness seems to result from two independent orientations of the dendritic moieties with respect to both the helical axis and macrocycle plane (fig. S11). Due to the chirality of the ethylene oxide chain, the oligoether dendron adopts an upward orientation irrespective of the expanded or contracted motif (Fig. 3A). However, the dendritic segments adopt different orientations with variation of the diameter of the helical tubule along the macrocycle plane. In the expanded motif, there are marginal spaces outside of the aromatic rings that the dendrimers occupy, resulting in steric repulsions between bulky dendritic segments on the left side of each vertex (Fig. 3B). To relieve the steric repulsions without sacrificing π -stacking interactions between the rods, the upper-layered macrocycles rotate clockwise to form left-handed helical tubules (Fig. 3D). However, in the contracted motif, the closely stacked macrocycles crowd out the dendrimers from the marginal space leading to steric crowding on the right side of each vertex (Fig. 3C). This spatial requirement induces the upper-layered macrocycles to rotate

counter clockwise, giving rise to right-handed helical tubules (Fig. 3E).

This dynamic motion of the tubules can be accompanied by packing variations of encapsulated hydrophobic guest molecules (Fig. 4). The tubules with aromatic cavities can take up C_{60} molecules through hydrophobic interactions during assembly. Upon addition of C_{60} to the solution of **2a**, the fluorescence intensity was considerably suppressed (Fig. 4A), indicating that C_{60} was effectively encapsulated within the hydrophobic interior of the tubules (26, 27). The fluorescence intensity decreased with an increase in fullerene content up to a certain point [0.8 equivalent (equiv.)], beyond which the fluorescence did not change upon further fullerene addition to the solution (Fig. 4A). Therefore, the maximum amount of C_{60} loading per bent-shaped molecule can be considered 0.8 equiv. On heating, a portion of the C_{60} guest population was released from the tubular interior due to the shrinkage of the tubules. The absorption intensity corresponding to C_{60} decreased to 0.4 equiv., indicating that 0.4 equiv. of C_{60} escape from the tubular interior through contraction (fig. S12). Subsequent cooling of the supernatant to room temperature led to a color change from dark to pale yellow, with considerably

Fig. 4. Encapsulation of fullerenes within the tubular cavities. **(A)** Fluorescence spectra ($\lambda_{\text{ex}} = 380$ nm) of **2a** in aqueous solution (0.05 wt %) without C_{60} and with 0.1 to 1.2 equiv. C_{60} . The inset shows the variation of emission intensity at 450 nm. **(B)** Ultraviolet-visible (UV-vis) spectra of **2a** and **2a**+ C_{60} in aqueous solution. The inset shows 10 \times magnified visible region. **(C)** UV-vis spectra of **2a** in aqueous solution with 0.4 equiv. C_{60} . **(D)** Reversible absorbance change of C_{60} inside tubular cavity upon temperature variation. **(E)** Schematic representation of the regulation of C_{60} - C_{60} interactions within the tubular cavities when the tubule contains 0.4 equiv of C_{60} .



reduced absorbance at 452 nm (Fig. 4C), indicating that C_{60} - C_{60} interactions are diminished due to expansion of the internal volume (28). The absorbance and solution color immediately recover to those of the contracted state upon subsequent heating, indicating that the breathing motion of the tubules leads to a reversible switch between tight and loose packing of the fullerenes within the tubular cavity (Fig. 4, D and E).

References and Notes

1. A. Klug, *Angew. Chem. Int. Ed. Engl.* **22**, 565 (1983).
2. J. L. Marx, *Science* **181**, 1236 (1973).
3. D. T. Bong, T. D. Clark, J. R. Granja, M. R. Ghadiri, *Angew. Chem. Int. Ed.* **40**, 988 (2001).
4. T. Shimizu, M. Masuda, H. Minamikawa, *Chem. Rev.* **105**, 1401 (2005).
5. J. P. Hill *et al.*, *Science* **304**, 1481 (2004).
6. V. Percec *et al.*, *Nature* **430**, 764 (2004).
7. H.-J. Kim *et al.*, *Angew. Chem. Int. Ed.* **49**, 8471 (2010).
8. D. M. Eisele, J. Knoester, S. Kirstein, J. P. Rabe, D. A. Vanden Bout, *Nat. Nanotechnol.* **4**, 658 (2009).
9. J. C. Nelson, J. G. Saven, J. S. Moore, P. G. Wolyne, *Science* **277**, 1793 (1997).
10. H. Shao *et al.*, *Angew. Chem. Int. Ed.* **49**, 7688 (2010).
11. M. R. Ghadiri, J. R. Granja, R. A. Milligan, D. E. McRee, N. Khazanovich, *Nature* **366**, 324 (1993).
12. M. Reches, E. Gazit, *Science* **300**, 625 (2003).
13. M. Iyoda, J. Yamakawa, M. J. Rahman, *Angew. Chem. Int. Ed.* **50**, 10522 (2011).
14. M. Schappacher, A. Deffieux, *Science* **319**, 1512 (2008).
15. F. F. Miranda *et al.*, *Small* **5**, 2077 (2009).
16. E. R. Ballister, A. H. Lai, R. N. Zuckermann, Y. Cheng, J. D. Mougous, *Proc. Natl. Acad. Sci. U.S.A.* **105**, 3733 (2008).
17. S. Hecht, A. Khan, *Angew. Chem. Int. Ed.* **42**, 6021 (2003).
18. M. C. Sicilia, A. Niño, C. Muñoz-Caro, *J. Phys. Chem. A* **109**, 8341 (2005).
19. K. Aidas, A. Maršalka, Z. Gdaniec, V. Balevičius, *Lithuanian J. Phys.* **47**, 443 (2007).
20. F. Würthner, T. E. Kaiser, C. R. Saha-Möller, *Angew. Chem. Int. Ed.* **50**, 3376 (2011).
21. B. W. Messmore, P. A. Sukerkar, S. I. Stupp, *J. Am. Chem. Soc.* **127**, 7992 (2005).
22. O. Henze *et al.*, *J. Am. Chem. Soc.* **128**, 5923 (2006).
23. J.-K. Kim, E. Lee, Y.-Lim, M. Lee, *Angew. Chem. Int. Ed.* **47**, 4662 (2008).
24. M. Peterca *et al.*, *J. Am. Chem. Soc.* **133**, 2311 (2011).
25. V. Percec, J. G. Rudick, M. Peterca, P. A. Heiney, *J. Am. Chem. Soc.* **130**, 7503 (2008).
26. M. Wolffs, F. J. M. Hoeben, E. H. A. Beckers, A. P. H. J. Schenning, E. W. Meijer, *J. Am. Chem. Soc.* **127**, 13484 (2005).
27. T. Yamaguchi, N. Ishii, K. Tashiro, T. Aida, *J. Am. Chem. Soc.* **125**, 13934 (2003).
28. G. D. Pantos, J.-L. Wietor, J. K. M. Sanders, *Angew. Chem. Int. Ed.* **46**, 2238 (2007).

Acknowledgments: We thank S. Lacher for helpful comments on the manuscript. This work was supported by the National Research Foundation of Korea (NRF) grant funded by the Korean government (MEST) (No. 2012-0001240). We acknowledge a fellowship of the BK21 program from the Ministry of Education and Human Resources Development.

Supplementary Materials

www.sciencemag.org/cgi/content/full/337/6101/1521/DC1
Materials and Methods
Supplementary Text
Figs. S1 to S12
References (29–37)

15 May 2012; accepted 9 August 2012
10.1126/science.1224741

A Crystalline Singlet Phosphinonitrene: A Nitrogen Atom–Transfer Agent

Fabian Dielmann,^{1,2} Olivier Back,¹ Martin Henry-Ellinger,^{1,2} Paul Jerabek,³ Gernot Frenking,³ Guy Bertrand^{1,2*}

A variety of transition metal–nitrido complexes (metallonitrenes) have been isolated and studied in the context of modeling intermediates in biological nitrogen fixation by the nitrogenase enzymes and the industrial Haber–Bosch hydrogenation of nitrogen gas into ammonia. In contrast, nonmetallic nitrenes have so far only been spectroscopically observed at low temperatures, despite their intermediacy in a range of organic reactions. Here, we report the synthesis of a bis(imidazolidin-2-iminato)phosphinonitrene, which is stable at room temperature in solution and can even be isolated in the solid state. The bonding between phosphorus and nitrogen is analogous to that observed for metallonitrenes. We also show that this nitrido phosphorus derivative can be used to transfer a nitrogen atom to organic fragments, a difficult task for transition metal–nitrido complexes.

Reactive intermediates play a central role in modern chemistry (1). The isolation of stable analogs has facilitated a better understanding of the reaction mechanisms and, in some cases, has given rise to distinct applications, as illustrated by the recent developments in carbene chemistry (2–7). However, there are still many families of reactive intermediates that

have eluded the synthetic skills of investigators: Among these are nitrenes (8, 9), the nitrogen analogs of carbenes, which are compounds with a neutral monocoordinate nitrogen atom featuring either a lone pair and two singly occupied non-

bonding orbitals (a triplet state) or two lone pairs and an accessible vacant orbital (a singlet state). These highly reactive electron-deficient species are involved in many reactions of synthetic interest such as CH-insertion, ring expansion, and aziridination processes but have never been isolated, with the exception of metallonitrenes **A** (Fig. 1A) (10–14). The latter can also be regarded as transition metal–nitrido complexes (L_nMN , where L is a ligand, and M is a metal), because one of their contributing resonance structures features a metal–nitrogen multiple bond. An M–N σ bond is formed from the interaction between an orbital of σ symmetry on the metal and a p_z or sp-hybrid orbital of the nitrogen atom. In addition, π bonds can be formed via overlap of the nitrogen p_x and p_y orbitals with appropriate orbitals of π symmetry on the metal. Overall, a metal–nitrogen bond order of three is possible.

The most stable nonmetallic nitrenes are the aminonitrenes **B** (Fig. 1B). The *N*-(2,2,5,5-tetramethylpyrrolidyl)nitrene (**B1**) and *N*-(2,2,6,6-tetramethylpiperidyl)nitrene (**B2**) (Fig. 1B) discovered by Dervan and co-workers (15–18) are sufficiently long lived in solution at -78°C to permit spectroscopic characterization and pu-

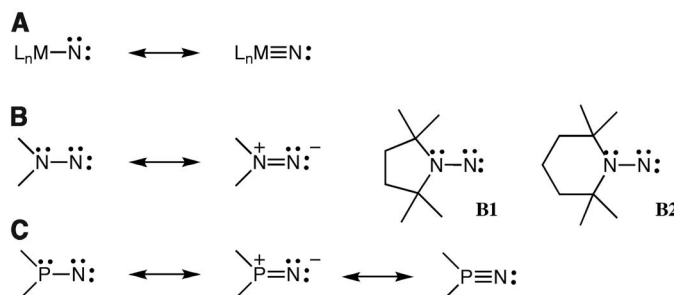


Fig. 1. Metallo- (A), amino- (B), and phosphinonitrenes (C) nitrenes (left) and their respective metal nitrido, 1,1-diazene, and phosphorus nitrido resonance forms (right). Aminonitrenes **B1** and **B2** are stable at low temperature.

¹University of California Riverside–CNRS Joint Research Chemistry Laboratory (UMI 2957), Department of Chemistry, University of California, Riverside, CA 92521–0403, USA. ²University of California San Diego–CNRS Joint Research Chemistry Laboratory (UMI 3555), Department of Chemistry and Biochemistry, University of California San Diego, La Jolla, CA 92093–0343, USA. ³Fachbereich Chemie, Philipps-Universität Marburg, Hans-Meerwein-Strasse, 35032 Marburg, Germany.

*To whom correspondence should be addressed. E-mail: guybertrand@ucsd.edu